Biochimica et Biophysica Acta 1818 (2012) 2120–2125

Contents lists available at SciVerse ScienceDirect

Biochimica et Biophysica Acta

journal homepage: www.elsevier.com/locate/bbamem

Hinge-bending motions in the pore domain of a bacterial voltage-gated sodium channel

Annika F. Barber [a,1], Vincenzo Carnevale [b,*,1], S.G. Raju [b,1], Cristiano Amaral [c], Werner Treptow [c], Michael L. Klein [b]

[a] Department of Neuroscience and Graduate Program in Cell and Developmental Biology, Thomas Jefferson University, Philadelphia, PA 19107, USA
[b] Institute for Computational Molecular Science, College of Science & Technology, Temple University, Philadelphia, PA 19122-6078, USA
[c] Laboratório de Biologia Teórica e Computacional, Departamento Biologia Celular, Universidade de Brasília, BR-70910-900 Brasília, DF, Brazil

ARTICLE INFO

Article history:
Received 23 December 2011
Received in revised form 11 April 2012
Accepted 2 May 2012
Available online 9 May 2012

Keywords:
Voltage gated
Sodium channel
Gating
NaChBac
Bacterial channel

ABSTRACT

Computational methods and experimental data are used to provide structural models for NaChBac, the homo-tetrameric voltage-gated sodium channel from the bacterium *Bacillus halodurans*, with a closed and partially open pore domain. Molecular dynamic (MD) simulations on membrane-bound homo-tetrameric NaChBac structures, each comprising six helical transmembrane segments (labeled S1 through S6), reveal that the shape of the lumen, which is defined by the bundle of four alpha-helical S6 segments, is modulated by hinge bending motions around the S6 glycine residues. Mutation of these glycine residues into proline and alanine affects, respectively, the structure and conformational flexibility of the S6 bundle. In the closed channel conformation, a cluster of stacked phenylalanine residues from the four S6 helices hinders diffusion of water molecules and Na^+ ions. Activation of the voltage sensor domains causes destabilization of the aforementioned cluster of phenylalanines, leading to a more open structure. The conformational change involving the phenylalanine cluster promotes a kink in S6, suggesting that channel gating likely results from the combined action of hinge-bending motions of the S6 bundle and concerted reorientation of the aromatic phenylalanine side-chains.

1. Introduction

Voltage-gated sodium channels (VGSCs) are responsible for the rising phase of the action potential in excitable cells, most notably in neurons and cardiac myocytes, where they play a critical role in neuronal firing and cardiac rhythm. Importantly, mutations in VGSC subunits have been implicated in an array of diseases including: paralysis, myotonia, epilepsy, arrhythmia and chronic neuropathic pain [1]. Notably, VGSCs are targets for drug molecules, including local anesthetics, painkillers, anticonvulsants and antiarrythmics [2], which bind to sites in the VGSC pore domain [3–5]. Moreover, many of these drugs show use-dependence, which reflects channel conformational dependent access to the relevant binding sites [6–9]. Accordingly, elucidating the functional conformations of the channel pore domain will allow a deeper understanding of the roles of VGSCs in physiology and disease.

Activation and inactivation are key voltage-dependent processes by which channels control ion conduction during the rising phase of the action potential. VGSCs preferentially adopt a non-conductive resting (closed) conformation at hyperpolarized transmembrane (TM) potentials. In response to membrane depolarization, VGSCs switch to their active (open) conformation, exhibiting high Na^+ ion conductance. Voltage-dependent activation is mediated by TM voltage sensor (VS) domains, each comprised four helical segments (S1 to S4). The VS is mechanically coupled to the pore domain (S5 and S6) via a linker region (S4–S5 linker). During activation, the S4 helix undergoes a conformational transition resulting in a net displacement towards the extracellular side of the membrane. During this process, a set of conserved arginines in S4 is involved in a sequential breaking and formation of salt bridges with the acidic residues of neighboring TM segments [10–17]. This conformational transition of the VS changes the position of the linker, which, in turn, induces a rearrangement of the S5 and S6 helical regions. Specifically, this process affects the structure of the helix bundle lining the pore and formed by four S6 helices from different subunits. Ultimately, the displacement of the linker results in the opening of the activation gate, a hydrophobic constriction region located at the crossing point of the four S6 segments [18–21]. Studies on NaChBac have postulated a mechanism, likely preserved in several VGSCs [22,23], in which this opening of the activation gate requires the S6 helix to form a kink at a conserved glycine [24,25]. As a probable ancestor of eukaryotic Na^+ and Ca^{2+} channels [26], NaChBac shares features of activation and gating with the mammalian counterparts. Interestingly, NaChBac also shows

* Corresponding author. Tel.: +1 215 204 4214.
E-mail address: vincenzo.carnevale@temple.edu (V. Carnevale).
[1] Contributed equally.

0005-2736/$ – see front matter © 2012 Elsevier B.V. All rights reserved.
doi:10.1016/j.bbamem.2012.05.002

sensitivity to mammalian VGSC inhibitors such as the local anesthetic etidocaine and the general anesthetic isoflurane [25,27].

Experimentally, activation and gating of VGSCs have received much attention [28]. However, thus far structural investigations have been limited by the size of the mammalian Na^+ channel pore-forming alpha subunit, which consists of twenty-four TM helices forming a pseudo-tetrameric structure. The discovery of homo-tetrameric bacterial VGSCs, each with just six TM helices [24,29,30] has provided an avenue for investigating VGSC gating behavior and structural characterization based on homology to known crystal structures of other tetrameric channels [31–33].

Here, we report a series of molecular dynamic (MD) studies on atomistic structural models of membrane-bound NaChBac based on the NavAb crystal structure. Our main focus of investigation is the characterization of structural properties of the TM S6-segment in different conformations of the channel. Accordingly, we present results on three channel conformations differing by the degree of openness at the activation gate and by the position of the VS-S4 helix.

Our modeling reveals that hinge bending motions around two S6-glycine residues of the channel are the key to modulating the shape of the main channel lumen. Specifically, a kink in S6 at G219 is related to pore opening; and another kink in S6, at G229, seems to favor the closure of the gate. In particular, a cluster of stacked phenylalanine residues in the crossing bundle of S6 helices, which hinder diffusion of water molecules and Na^+ ions in the closed pore domain experimental VGSC structure, is critical for the gating process, working together as a major hydrophobic gate on the ionic permeation pathway. Overall, the present MD study identifies the S6-glycines as the crucial molecular hinge points, accounting for the bending motions of the S6 segment, which are associated with VS activation leading to channel opening. We thus hypothesize that these S6-glycines are key players in the mechanism of pore opening and closing during the voltage-gating process.

2. Methods

2.1. Modeling the closed conformation

A structural model for NaChBac in a closed conformation was built starting from the X-ray crystal structure of NavAb (PDB ID: 3RVY), which was crystallized in a closed-pore conformation with the four VS domains partially activated. The VGSCs, NaChBac and NavAb are closely related, sharing significant levels of sequence identity (~37%) (Fig. S1). Ten residues at the N-terminus of NaChBac are not present in NavAb and were not included in the model. Five additional residues at the C-terminal region of NaChBac, predicted to be in an alpha-helical configuration by PSIPRED [34] and not resolved in the X-ray structure of NavAb, were added to the structure. We used MODELLERv9 [35] to generate the NaChBac structural homology model.

After energy minimization, the model for NaChBac in a closed conformation was embedded in a fully hydrated lipid bilayer for subsequent equilibration by MD simulation. The homotetrameric channel was inserted at the center of a 1-palmitoyl-2-oleoyl-sn-glycero-3-phosphocholine (POPC) lipid patch. To generate the initial configuration, a set of conserved aromatic side-chains was used as a guide to delimit the TM region of the bilayer. The macromolecular system contained a total of ~162,000 atoms, including NaChBac, 434 lipid molecules, 28173 water molecules and 232 ions in solution. Two Na^+ ions were initially placed in the channel SF, at sites HFS and IN (Fig. 1), in agreement with a previous computational study of NavAb showing double occupancy of the filter by Na^+ ions [36]. All charged amino acids were simulated in their fully ionized state (pH = 7.0).

The membrane-bound channel system was relaxed following two consecutive steps: (i) membrane equilibration for ~10.0 ns with the channel backbone coordinates restrained around their starting structure with a harmonic force constant of 1 kcal/mol/Å^2. This procedure ensured a uniform and tight distribution of lipid molecules around the protein without perturbing the initial conformation; and (ii) 0.3 μs relaxation of the full channel system by means of unconstrained MD simulation. Starting from the relaxed structure of the wild type (WT), additional unconstrained MD simulations were performed on two mutants, G219P and G219A. For each mutant a trajectory of 0.15 μs was collected for subsequent analysis.

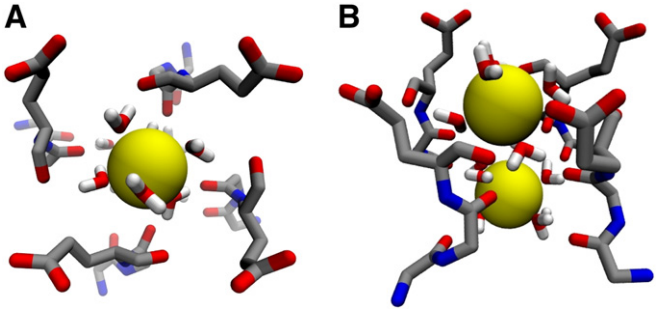

Fig. 1. Structure of the selectivity filter with two solvated Na^+ ions: (A) upper view from the outer vestibule; (B) side-view. Main chain groups from residues Thr189, Leu190 and Glu191 and the side-chain of Glu191 plus water molecules are shown in stick representation, while Na^+ ions are rendered as yellow spheres.

2.2. Modeling the early-activated-open conformation

Starting from the closed structure of NaChBac, we generated the pre-open conformation of the channel by means of a steered-MD protocol, which mimics the iris-like dilation mechanism recently proposed for pore opening of the channel [37]. In our protocol, the S6-helical bundle was splayed apart by applying time-dependent harmonic potentials (force constant of 5 kcal/mol/Å^2) along 16 inter-subunit distances, defined between the C-alpha atoms of the four pore-lining S6 residues F224, I228, I231 and R234. The time-dependent restraints were applied over a 40 ns MD run until the inter-subunit distances approximated the corresponding ones in the open structure of Kv1.2/2.1. After these restraints were satisfied, solvation of the channel lumen and free diffusion of Na^+ ions across the activation gate were observed. We then launched a restraint-free 0.300 μs MD trajectory for the membrane-bound channel, which allowed extensive assessment of the structural properties of the channel in a “pre-open” conformation.

2.3. Modeling the activated-partially-open conformation

Starting from the structure of the closed conformation of NaChBac, a model of the activated conformation was built via a steered-MD approach. Harmonic restraints were applied to the center of mass of the voltage-sensing S4 helix and the equilibrium position was shifted over time so as to induce a 6-Å rigid-body motion of the helix over an MD trajectory spanning 70 ns. The choice of a 6-Å displacement is based on an a priori inspection of the VS domain of Kv1.2–2.1. To preserve the alpha-helical conformation and prevent unfolding of the S4 helix, additional restraints were applied to all the main-chain H-bonds within the helical segment, which spans from residues 110 to 126. The total displacement of S4 is the minimal distance allowing interaction between R4 and D60, a salt-bridge shown to be present in the fully activated state [37]. To explore the effect of a depolarizing potential on this partially activated conformation, an additional 0.270 μs MD trajectory was sampled with an imposed TM potential of 1 V, which was applied through the addition of an external uniform electrostatic field.

2.4. Molecular dynamic simulations

All MD simulations used the CHARMM22-CMAP force field with torsional cross-terms for the protein and CHARMM27 for the phospholipids [38,39]. A united-atom representation was adopted for the acyl chains of the POPC lipid molecules [40]. The water molecules were described using the TIP3P model [41,42]. Periodic boundary conditions were employed for all of the MD simulations and the electrostatic potential was evaluated using the particle-mesh Ewald method [43]. The lengths of all bonds containing hydrogen were constrained with the SHAKE algorithm [44]. The system was maintained at a temperature of 300 K and pressure of 1 atm using the Langevin thermostat and barostat methods as implemented in the MD code NAMD2.7 [45], which was used for the simulations with a 2.0 fs time step.

2.5. Free-energy calculations

The free-energy profile or potential of mean force (PMF) of ion conduction was calculated using the adaptive-biasing-force (ABF) method implemented in NAMD [42,46]. Here, we followed a similar strategy previously described to compute the free energy associated with the ion conduction through voltage-gated potassium channels [21]. In brief, the reaction coordinate for conduction through the activation gate was defined as the distance between the ion and the geometric center of the TLESW motif at the selectivity filter. For the early-activated-open conformation, the translocation of the ion follows a path of length 15 Å, ranging from the cytoplasmic entrance of the pore to the entrance of the central cavity, located immediately above the residue F224. The free-energy profile was calculated by means of independent MD runs, each exploring a 5-Å section of the reaction coordinate.

3. Results and discussion

Three models of NaChBac were built on the basis of the recently determined X-ray crystal structure of the closely related NavAb channel [47] presenting the VS in different stages of activation [12–17], each exhibiting a well-defined electrostatic network between basic amino acids of the helical S4-segment and the acidic binding sites within the domain (Fig. 2). Of note are two salt-bridges (R2-E43 and R3-D60) and the 3_{10}-helix conformation of the S4 segment encompassing R3 and R4, which have been shown to be the structural determinants of at least one of the activated conformations of the VSD [37]. Remarkably, the cavities, called fenestrations, which connect the pore lumen to the hydrophobic region of the lipid bilayer are present in all the conformations explored along the MD trajectories and do not experience significant structural rearrangements. In contrast, the main-pore regions differ considerably in the degree of openness of the ionic-conduction pathway with the pore ranging from a closed to an open conformation.

For all models, the root mean square deviation (RMSD) values for the whole channel as well as for the VS and pore domains range from 1.5 to 4 Å (Fig. 3), which is typical of the structural drift quantified in previous MD simulation studies of ion channels [48,49]. The activated-partially-open conformation has the largest RMSD due to the relaxation of the VS on removal of the constraints. To further evaluate the model we compared interatomic distances for 9 specific residue pairs in the final membrane-equilibrated structure of the early-activated-open conformation (Table S1) to distances estimated from luminescence resonance energy transfer (LRET) measurements for these pairs [31]. We found variations of less than 5.4 Å, a result consistent with previously published models of NaChBac [26,33].

The major structural differences between the conformations of the pore domain are found in the pore-lining S6 helices. In the closed conformation, below the SF, the channel pore features a large hydrated central cavity, disconnected from the intracellular aqueous environment by a cluster of S6-phenylalanine residues, F224 and F227, located at the activation gate region (Fig. 4A–B). These phenylalanine side chains project into the channel lumen, producing inter-subunit stacking interactions, thereby occluding the pore. In contrast, in the early-activated-open conformation, the F224 side chains are buried in the inter-subunit helical interface rather than being stacked in the lumen, and pairs of F227 side chains interact in an "edge-face" conformation (Fig. 4A–B). The latter arrangement of the phenylalanine cluster allows hydration of the activation gate, a key structural modification required for ionic transportation [21]. The free-energy profile associated with conduction of Na^+ through the activation gate of the early-activated-open conformation shows an energy barrier of ~15 kcal/mol (Fig. S2), indicating that, although the permeant Na^+ ion retains an almost intact shell of solvation, the structure is not fully open for diffusive transport. However, this barrier is significantly smaller than the energy cost (~50 kcal/mol) estimated for ion translocation across the closed gate of homologous voltage-gated K^+ channels [21] suggesting the early-activated-open conformation as an intermediate partially open structure on the closed-to-open transition pathway of NaChBac.

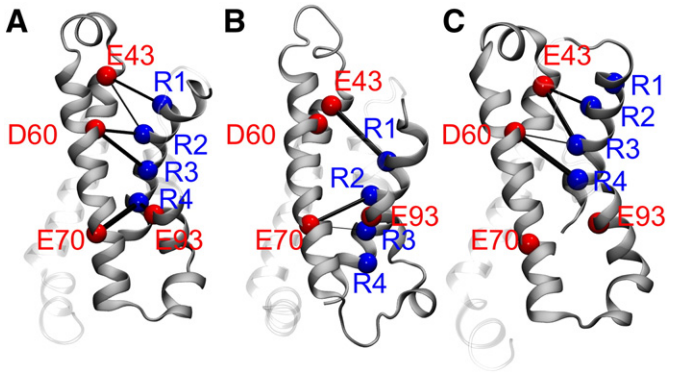

Fig. 2. Shown are the patterns of salt-bridges in the voltage-sensing domain (VSD) of NaChBac for selected conformations of the channel: (A) closed; (B) early-activated-open; and (C) activated-partially-open (see text). The C-alpha atoms of the arginines and the acidic residues of the VSD are shown as blue and red spheres, respectively. The thickness of the black cylinders reflects the relative occurrence of each salt-bridge along the MD simulation trajectory.

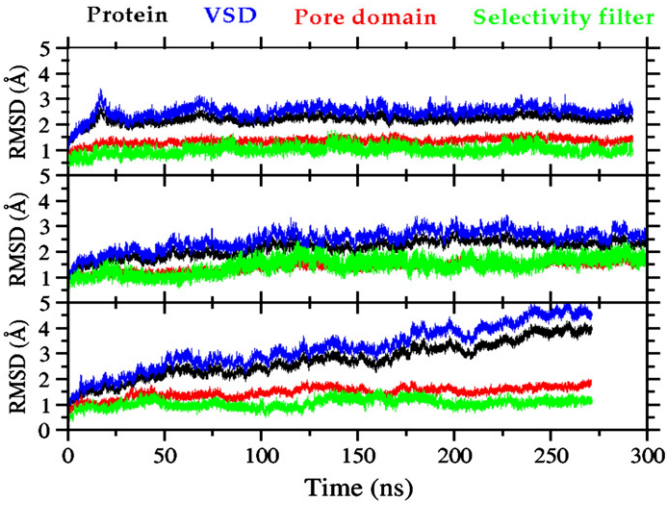

Fig. 3. Root mean square deviation (RMSD) of the backbone atoms from the initial structure employed in the MD simulation plotted as a function of time for: (A) closed; (B) early-activated-open; and (C) activated-partially-open conformations, respectively (see text). The RMSD is shown separately for different regions of the channel: entire channel (black), voltage-sensing domains (blue), pore domain (red), and selectivity filter (green).

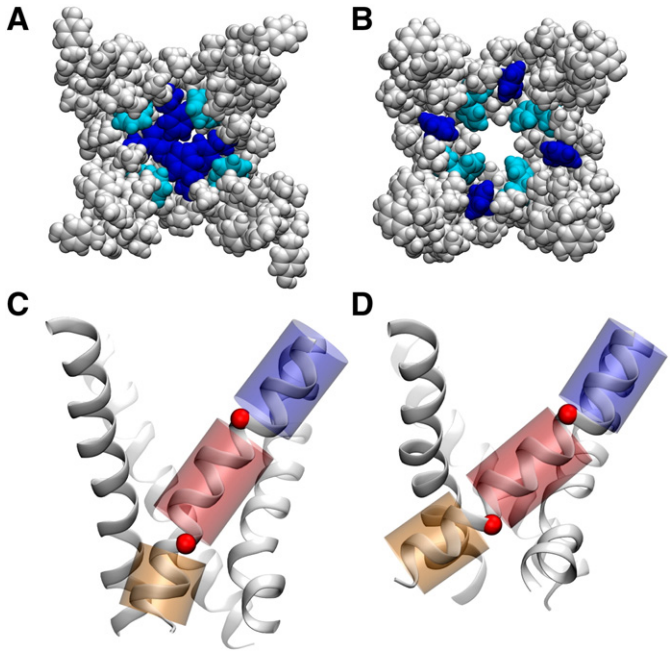

Fig. 4. Conformations of the NaChBac pore domain along the activation pathway as determined in the present study, with only the S6-helix bundle shown for clarity. Upper panels: (A, B) space-filling representation of the channel lumen for the closed and activated-partially-open conformations, respectively. Phenyl groups Phe224 and Phe227 are shown in blue and cyan, respectively. Bottom panels: (C, D) cartoon representation of the S6-helix bundle highlighting the hinge-bending motions around residues G219 and G229 (red spheres) involving the three helical regions (blue, red, and orange) for the closed and activated-partially-open conformations, respectively.

The presence of two glycine residues endows the S6-helix with conformational flexibility at positions 219 and 229 and suggests a mechanism underlying pore domain gating transitions in which these glycine residues act as hinges and decouple the motions of the three resulting helical regions (Fig. 4C–D). Notably the angle at position 219 is considerably different between the two conformations (Fig. 5). On passing from closed- to open-pore, the kink angle between the two helical segments upstream and downstream of G219 (residues 210–218 and 220–228) changes from an average value of 10° to 20° (Fig. 5). The opposite behavior is observed for the kink angle at position 229 (defined as the angle between the helical regions 218–228 and 230–240), for which a more pronounced kink is found in this case for the closed conformation: 20° and 10°, for closed and open, respectively.

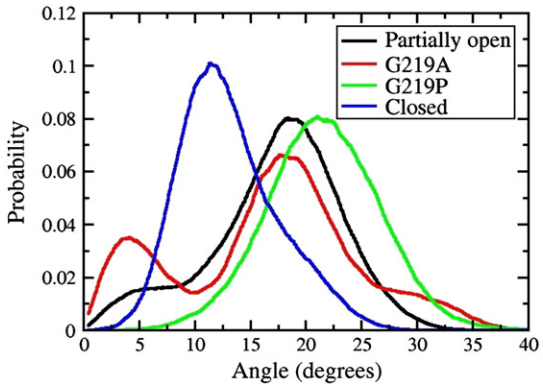

Fig. 5. Probability distributions of S6 kink angles around G219 (A) and G229 (B) for the activated-partially-open (black) and closed (blue) conformations, along with results for the mutants G219A (red) and G219P (green). The angles are measured between the helical segments adjacent to the glycine residues: segments 210–218 and 220–228 for G219 and 218–228 and 230–240 for G229.

The rigid-body motions of these helical S6-segments modulate the packing at the inter-subunit interfaces, which in turn, determine the shape of the pore. Indeed an increased tilt of the C-term region of S6 allows the four S6 helices to be splayed apart, which results in an expansion of the constriction region located at the phenylalanine cluster (Fig. 4A–B). Therefore a stable kink at position 219 is seemingly the structural determinant of the *open* state. Moreover, this structural feature is consistent with mutagenesis data [24] showing that the G219A mutant, with decreased flexibility at position 219, inactivates faster than the WT. The data suggest that a significant destabilization of the *open* state can be achieved by decreasing the propensity of S6 for kinked configurations. Furthermore, independent experimental studies have shown that mutation of G219 into proline stabilizes a kinked S6-segment, and therefore the *open* conformation [25].

Additional independent MD simulations were performed on the G219P and G219A mutants to characterize the effect of these mutations on the kink propensity and bending flexibility of the S6-segment. The most dramatic effect is observed for the proline mutant: compared to the WT, where the distribution of kink angles shifts significantly toward larger values (Fig. 5). Furthermore, configurations featuring angles smaller than 10° are never explored. As expected, the less perturbing mutation of glycine into alanine results in smaller differences compared to the WT: two peaks are apparent in the distribution around 5° and 20°, respectively corresponding to the straight and kinked configurations (Fig. 5). Despite showing a slightly decreased probability for kinked configurations, the distribution is very similar to that of the WT, suggesting that mutation of glycine into alanine at position 219 does not dramatically affect the overall structure of the S6 bundle and that the increased rate of inactivation may result from the slightly decreased conformational flexibility.

To further characterize the role of the phenylalanine cluster, we investigated the early events of the gating transition. To this end, we have modeled a conformation featuring fully activated VS domains and monitored the response of the pore over a time-scale of 0.270 μs. Simulations were started from the closed-pore configuration and S4 helix was moved to the fully activated state (as described in Ref. [37]) by means of steered MD. As expected, the most relevant structural rearrangement occurs at the S4–S5 linker, where the helical region of the linker is displaced by 6 Å along the normal to the membrane surface (Fig. 6). As a result, the steric constraints on the bundle-crossing region of S6 are weaker than in the early-activated state and in-plane movements of the C-term region of S6 are less restricted. It is worth noting that this configuration of the S4–S5 linker is coupled to a conformational change in the S6 bundle. Specifically, an increased tilt of the N-term region of S6 allows the helices to be splayed apart without the need for a kink at position 219. Although the S6 bundle was not able to reach the fully open conformation over the relatively short MD time-scale, a significant rearrangement was observed in the phenylalanine cluster: rather than being stacked in the pore-lumen, the bulky aromatic side-chains are found, on average, to be buried in the helix–helix interfaces in configurations remarkably similar to those found in the early-activated-open state.

The major consequence of the above-mentioned rearrangement is the inability of the cluster of phenylalanines to act as a hydrophobic seal preventing waters, and thus solvated ions, from traversing the bundle cross. Over the course of simulation we observe sufficient opening to allow water flux in the presence of a TM potential. This change in hydration can be seen in Fig. 7 in which the intermittent formation of water wires spanning the entire pore is highlighted by the presence of density in the −7 Å to −15 Å region. The ability of water molecules to occupy this section of the pore suggests that hydration of the hydrophobic constriction region may be the early response to activation leading to destabilization of the closed conformation and inducing, ultimately, the conformational transition to the fully open state.

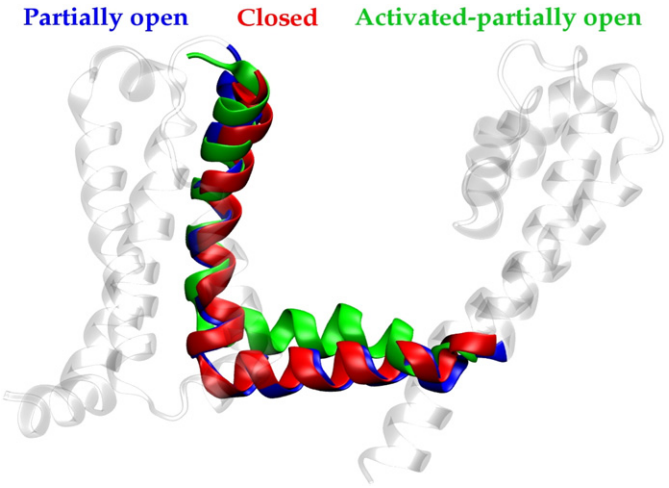

Fig. 6. Shown is a superposition of structures of the NaChBac S4–S5 linker for closed (red), early-activated-open (blue) and activated-partially-open (green) conformations (see text), highlighting the displacement of the linker along the direction normal to the membrane.

In light of our observations, the following activation scheme can be envisioned for NaChBac: in response to VS activation, the S4–S5 linker cuff is displaced along the normal to the membrane; this movement increases the tilt of the coupled C-term regions of S6 helices and thus induces an expansion of the bundle. A flexible hinge movement at G219 facilitates this conformational transition and results in an opening of the pore.

4. Conclusions

The bacterial Na^+ channel NaChBac is evolutionarily related to eukaryotic Na^+ channels and [26,29] has been the subject of extensive experimental and computational investigations [10,12–14,17,24,25,31–33,50,51] aimed at revealing general mechanistic aspects of gating in VGSCs. The structural rearrangement of the pore domain during the gating process is one of the most significant issues to be addressed due to the role of the pore in binding a number of clinically relevant drugs. The present computational study builds upon extensive experimental data and previously derived models of NaChBac gating [12–14,17,52] to reveal significant conformational changes in the S6 pore-lining helix bundle during gating.

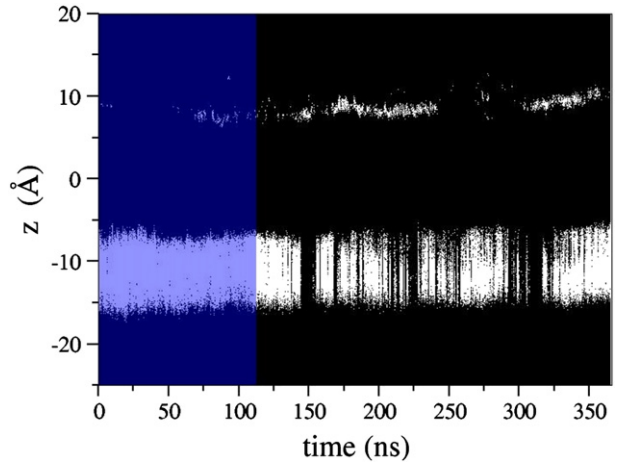

Fig. 7. Shown are the positions of water oxygen atoms projected onto the membrane normal (Z). Blue shading highlights the portion of the MD trajectory sampled before an external electrostatic field was applied. Under the electric field, the frequency of wetting/dewetting transitions at the hydrophobic gate (located approximately between −7 Å and −15 Å) increases dramatically.

By comparing structural models of the closed, early-activated-open, and activated-partially-open conformations of the channel, we identify hinge-bending motions around two glycine residues in S6, which are able to modulate the shape of the channel lumen along the activation pathway. Specifically, starting from the closed state, a tilt of the C-term region of S6 allows pore opening and induces the formation of a kink at position 219; full activation of the VS domains entails a structural rearrangement of the linker, which, in turn, is coupled to tilting of the N-term region of S6 and a relaxation from the kinked to the unkinked state. Significantly, a cluster of stacked phenylalanine residues in the pore, which hinder diffusion of water molecules and Na^+ ions in the resting and activated-closed states, undergoes a structural rearrangement upon expansion of the S6 helical bundle in the open state. This scheme is in agreement with previous structural descriptions of hydrophobic-gate controlled mechanisms of ion conduction in other channels [53–57].

In addition to creating structural models of NaChBac that will be useful for investigating interactions with commonly used VGSC-modulatory drugs, our findings suggest interesting features of the pore domain that merit experimental investigation: the function of gate phenylalanines, the nature of VS-gate coupling, and the role of fenestrations in gating and drug access to internal sites. The hydrophobic seal formed by phenylalanines is not found in the NavAb crystal structure and thus also demands further experimental investigation. Mutation of these residues could cause shifts in voltage dependence by changing the ease of opening the gate. Additionally, mutation to charged residues could create constitutively open or closed channels. How the movement of these phenylalanines is energetically coupled to VS conformational changes can also be explored by mutational analysis.

The fenestrations found in the NavAb crystal structure are preserved in the NaChBac homology model in all of the explored conformations. These fenestrations have not been seen in other tetrameric channel crystal structures, but may play a role in allowing pore domain flexibility necessary for gating and could also provide an access path for drugs. Mutations that occlude the fenestrations would permit investigation of whether they are necessary for gating and the observation that they are permanently open in all the conformations examined reinforces the hypothesis that small drugs could reach internal sites via fenestrations. Further investigation of drug access pathways through fenestrations and a search for fenestration-like formations in mammalian VGSC sequences via further modeling and electrophysiological experimentation will be necessary to determine whether they represent the “lipophilic” pathway proposed by Hille [6,9].

Given that the action of VGSC modulating drugs is known to shift the relative stability of specific gating conformations [3,4,27,58–64] our structures will enable further computational investigations, which will likely shed light on the nature of drug binding modalities in NaChBac as well as the more general issue of the mechanism of drug-sensitivity of VGSCs.

Acknowledgements

We are grateful for support from the National Institutes of Health, and the Commonwealth of Pennsylvania. We also thank Manuel Covarrubias for very useful scientific discussion. A.F.B. acknowledges the National Institutes of Health (grants NIH-NIAAA T32 AA007463 and NIH-NINDS F31 NS077689) for financial support. The National Science Foundation supported this work through XSEDE resources provided by the National Institute for Computational Sciences (grant TG-MCA93S020).

Appendix A. Supplementary data

Supplementary data to this article can be found online at http://dx.doi.org/10.1016/j.bbamem.2012.05.002.

References

[1] A.L. George, Inherited disorders of voltage-gated sodium channels, J. Clin. Invest. 115 (2005) 1990–1999.
[2] J.J. Clare, S.N. Tate, M. Nobbs, M.A. Romanos, Voltage-gated sodium channels as therapeutic targets, Drug Discov. Today 5 (2000) 506–520.
[3] D.S. Ragsdale, J.C. McPhee, T. Scheuer, W.A. Catterall, Molecular determinants of state-dependent block of Na^+ channels by local anesthetics, Science 265 (1994) 1724–1728.
[4] D.S. Ragsdale, J.C. McPhee, T. Scheuer, W.A. Catterall, Common molecular determinants of local anesthetic, antiarrhythmic, and anticonvulsant block of voltage-gated Na^+ channels, Proc. Natl. Acad. Sci. U. S. A. 93 (1996) 9270–9275.
[5] V. Yarov-Yarovoy, J.C. McPhee, D. Idsvoog, C. Pate, T. Scheuer, W.A. Catterall, Role of amino acid residues in transmembrane segments IS6 and IIS6 of the Na^+ channel alpha subunit in voltage-dependent gating and drug block, J. Biol. Chem. 277 (2002) 35393–35401.
[6] B. Hille, Local anesthetics: hydrophilic and hydrophobic pathways for the drug–receptor reaction, J. Gen. Physiol. 69 (1977) 497–515.
[7] G.R. Strichartz, The inhibition of sodium currents in myelinated nerve by quaternary derivatives of lidocaine, J. Gen. Physiol. 62 (1973) 37–57.
[8] K.R. Courtney, Mechanism of frequency-dependent inhibition of sodium currents in frog myelinated nerve by the lidocaine derivative GEA, J. Pharmacol. Exp. Ther. 195 (1975) 225–236.
[9] B. Hille, Ion Channels of Excitable Membranes, Sinauer, Sunderland, Mass., 2001
[10] A. Kuzmenkin, F. Bezanilla, A.M. Correa, Gating of the bacterial sodium channel, NaChBac: voltage-dependent charge movement and gating currents, J. Gen. Physiol. 124 (2004) 349–356.
[11] J. Blanchet, S. Pilote, M. Chahine, Acidic residues on the voltage-sensor domain determine the activation of the NaChBac sodium channel, Biophys. J. 92 (2007) 3513–3523.
[12] P.G. DeCaen, V. Yarov-Yarovoy, Y. Zhao, T. Scheuer, W.A. Catterall, Disulfide locking a sodium channel voltage sensor reveals ion pair formation during activation, Proc. Natl. Acad. Sci. U. S. A. 105 (2008) 15142–15147.
[13] P.G. DeCaen, V. Yarov-Yarovoy, E.M. Sharp, T. Scheuer, W.A. Catterall, Sequential formation of ion pairs during activation of a sodium channel voltage sensor, Proc. Natl. Acad. Sci. U. S. A. 106 (2009) 22498–22503.
[14] T. Paldi, M. Gurevitz, Coupling between residues on S4 and S1 defines the voltage-sensor resting conformation in NaChBac, Biophys. J. 99 (2010) 456–463.
[15] W.A. Catterall, Ion channel voltage sensors: structure, function, and pathophysiology, Neuron 67 (2010) 915–928.
[16] T. Shimomura, K. Irie, H. Nagura, T. Imai, Y. Fujiyoshi, Arrangement and mobility of the voltage sensor domain in prokaryotic voltage-gated sodium channels, J. Biol. Chem. 286 (2011) 7409–7417.
[17] P.G. Decaen, V. Yarov-Yarovoy, T. Scheuer, W.A. Catterall, Gating charge interactions with the S1 segment during activation of a Na^+ channel voltage sensor, Proc. Natl. Acad. Sci. U. S. A. 108 (2011) 18825–18830.
[18] D.A. Doyle, J.M. Cabral, R.A. Pfuetzner, A. Kuo, J.M. Gulbis, S.L. Cohen, B.T. Chait, R. MacKinnon, The structure of the potassium channel: molecular basis of K^+ conduction and selectivity, Science 280 (1998) 69.
[19] C. Townsend, R. Horn, Interaction between the pore and a fast gate of the cardiac sodium channel, J. Gen. Physiol. 113 (1999) 321–332.
[20] C.C. Kuo, S.Y. Liao, Facilitation of recovery from inactivation by external Na^+ and location of the activation gate in neuronal Na^+ channels, J. Neurosci. 20 (2000) 5639–5646.
[21] W. Treptow, M. Tarek, Environment of the gating charges in the Kv1.2 Shaker potassium channel, Biophys. J. 90 (2006) L64–L66.
[22] Y. Jiang, A. Lee, J. Chen, V. Ruta, M. Cadene, B.T. Chait, R. MacKinnon, X-ray structure of a voltage-dependent K^+ channel, Nature 423 (2003) 33–41.
[23] S.M. Webster, D. Del Camino, J.P. Dekker, G. Yellen, Intracellular gate opening in Shaker K^+ channels defined by high-affinity metal bridges, Nature 428 (2004) 864–868.
[24] K. Irie, K. Kitagawa, H. Nagura, T. Imai, T. Shimomura, Y. Fujiyoshi, Comparative study of the gating motif and C-type inactivation in prokaryotic voltage-gated sodium channels, J. Biol. Chem. 285 (2010) 3685–3694.
[25] Y. Zhao, T. Scheuer, W.A. Catterall, Reversed voltage-dependent gating of a bacterial sodium channel with proline substitutions in the S6 transmembrane segment, Proc. Natl. Acad. Sci. U. S. A. 101 (2004) 17873–17878.
[26] K. Charalambous, B.A. Wallace, NaChBac: the long lost sodium channel ancestor, Biochemistry 50 (2011) 6742–6752.
[27] W. OuYang, H.C. Hemmings, Isoform-selective effects of isoflurane on voltage-gated Na^+ channels, Anesthesiology 107 (2007) 91–98.
[28] W.A. Catterall, From ionic currents to molecular mechanisms: the structure and function of voltage-gated sodium channels, Neuron 26 (2000) 13–25.
[29] D. Ren, B. Navarro, H. Xu, L. Yue, Q. Shi, D.E. Clapham, A prokaryotic voltage-gated sodium channel, Science 294 (2001) 2372–2375.
[30] R. Koishi, H. Xu, D. Ren, B. Navarro, B.W. Spiller, Q. Shi, D.E. Clapham, A superfamily of voltage-gated sodium channels in bacteria, J. Biol. Chem. 279 (2004) 9532–9538.
[31] J. Richardson, R. Blunck, P. Ge, P.R. Selvin, F. Bezanilla, D.M. Papazian, A.M. Correa, Distance measurements reveal a common topology of prokaryotic voltage-gated ion channels in the lipid bilayer, Proc. Natl. Acad. Sci. U. S. A. 103 (2006) 15865–15870.
[32] Y. Shafrir, S.R. Durell, H.R. Guy, Models of the structure and gating mechanisms of the pore domain of the NaChBac ion channel, Biophys. J. 95 (2008) 3650–3662.
[33] Y. Shafrir, S.R. Durell, H.R. Guy, Models of voltage-dependent conformational changes in NaChBac channels, Biophys. J. 95 (2008) 3663–3676.
[34] D.T. Jones, Protein secondary structure prediction based on position-specific scoring matrices1, J. Mol. Biol. 292 (1999) 195–202.
[35] A. Fiser, A. Sali, Modeller: generation and refinement of homology-based protein structure models, Methods Enzymol. 374 (2003) 461–491.
[36] V. Carnevale, W. Treptow, M.L. Klein, Sodium ion binding sites and hydration in the lumen of a bacterial ion channel from molecular dynamic simulations, J. Phys. Chem. Lett. 109 (2011) E93–E102.
[37] V. Yarov-Yarovoy, P.G. Decaen, R.E. Westenbroek, C.Y. Pan, T. Scheuer, D. Baker, W.A. Catterall, Structural basis for gating charge movement in the voltage sensor of a sodium channel, Proc. Natl. Acad. Sci. U. S. A. 2 (2011) 2504–2508.
[38] A.D. MacKerell, N. Banavali, N. Foloppe, Development and current status of the CHARMM force field for nucleic acids, Biopolymers 56 (2000) 257–265.
[39] A.D. Mackerell, M. Feig, C.L. Brooks, Extending the treatment of backbone energetics in protein force fields: limitations of gas-phase quantum mechanics in reproducing protein conformational distributions in molecular dynamic simulations, J. Comput. Chem. 25 (2004) 1400–1415.
[40] J. Hénin, W. Shinoda, M.L. Klein, United-atom acyl chains for CHARMM phospholipids, J. Phys. Chem. B 112 (2008) 7008–7015.
[41] W.L. Jorgensen, J. Chandrasekhar, J.D. Madura, R.W. Impey, M.L. Klein, Comparison of simple potential functions for simulating liquid water, J. Chem. Phys. 79 (1983) 926.
[42] E. Darve, D. Rodríguez-Gómez, A. Pohorille, Adaptive biasing force method for scalar and vector free energy calculations, J. Chem. Phys. 128 (2008) 144120.
[43] U. Essmann, L. Perera, M.L. Berkowitz, T. Darden, H. Lee, L.G. Pedersen, A smooth particle mesh Ewald method, J. Chem. Phys. 103 (1995) 8577.
[44] J.P. Ryckaert, G. Ciccotti, H.J.C. Berendsen, Numerical integration of the cartesian equations of motion of a system with constraints: molecular dynamics of n-alkanes, J. Comput. Phys. 23 (1977) 327–341.
[45] J.C. Phillips, R. Braun, W. Wang, J. Gumbart, E. Tajkhorshid, E. Villa, C. Chipot, R.D. Skeel, L. Kale, K. Schulten, Scalable molecular dynamics with NAMD, J. Comput. Chem. 26 (2005) 1781–1802.
[46] J. Henin, G. Fiorin, C. Chipot, M.L. Klein, Exploring multidimensional free energy landscapes using time-dependent biases on collective variables, J. Chem. Theory Comput. 6 (2009) 35–47.
[47] J. Payandeh, T. Scheuer, N. Zheng, W.A. Catterall, The crystal structure of a voltage-gated sodium channel, Nature 475 (2011) 353–358.
[48] S. Berneche, B. Roux, Molecular dynamics of the KcsA K^+ channel in a bilayer membrane, Biophys. J. 78 (2000) 2900–2917.
[49] I.H. Shrivastava, M.S.P. Sansom, Simulations of ion permeation through a potassium channel: molecular dynamics of KcsA in a phospholipid bilayer, Biophys. J. 78 (2000) 557–570.
[50] E. Pavlov, C. Bladen, R. Winkfein, C. Diao, P. Dhaliwal, R.J. French, The pore, not cytoplasmic domains, underlies inactivation in a prokaryotic sodium channel, Biophys. J. 89 (2005) 232–242.
[51] L. Yue, B. Navarro, D. Ren, A. Ramos, D.E. Clapham, The cation selectivity filter of the bacterial sodium channel, NaChBac, J. Gen. Physiol. 120 (2002) 845.
[52] S. Chakrapani, P. Sompornpisut, P. Intharathep, B. Roux, E. Perozo, The activated state of a sodium channel voltage sensor in a membrane environment, Proc. Natl. Acad. Sci. U. S. A. 107 (2010) 5435–5440.
[53] T. Kitaguchi, M. Sukhareva, K.J. Swartz, Stabilizing the closed S6 gate in the Shaker Kv channel through modification of a hydrophobic seal, J. Gen. Physiol. 124 (2004) 319–332.
[54] Y. Jiang, A. Lee, J. Chen, M. Cadene, B.T. Chait, R. MacKinnon, The open pore conformation of potassium channels, Nature 417 (2002) 523–526.
[55] J.N. Bright, I.H. Shrivastava, F.S. Cordes, M.S. Sansom, Conformational dynamics of helix S6 from Shaker potassium channel: simulation studies, Biopolymers 64 (2002) 303–313.
[56] S.A. Spronk, D.E. Elmore, D.A. Dougherty, Voltage-dependent hydration and conduction properties of the hydrophobic pore of the mechanosensitive channel of small conductance, Biophys. J. 90 (2006) 3555–3569.
[57] B. Corry, An energy-efficient gating mechanism in the acetylcholine receptor channel suggested by molecular and Brownian dynamics, Biophys. J. 90 (2006) 799–810.
[58] M. Shiraishi, R.A. Harris, Effects of alcohols and anesthetics on recombinant voltage-gated Na^+ channels, J. Pharmacol. Exp. Ther. 309 (2004) 987–994.
[59] W. Ouyang, T.Y. Jih, T.T. Zhang, A.M. Correa, H.C. Hemmings, Isoflurane inhibits NaChBac, a prokaryotic voltage-gated sodium channel, J. Pharmacol. Exp. Ther. 322 (2007) 1076–1083.
[60] H.C. Hemmings, Sodium channels and the synaptic mechanisms of inhaled anaesthetics, Br. J. Anaesth. 103 (2009) 61–69.
[61] S.D. Dib-Hajj, J.A. Black, S.G. Waxman, Voltage-gated sodium channels: therapeutic targets for pain, Pain Med. 10 (2009) 1260–1269.
[62] M. Mantegazza, G. Curia, G. Biagini, D.S. Ragsdale, M. Avoli, Voltage-gated sodium channels as therapeutic targets in epilepsy and other neurological disorders, Lancet Neurol. 9 (2010) 413–424.
[63] C.J. Cohen, Targeting voltage-gated sodium channels for treating neuropathic and inflammatory pain, Curr. Pharm. Biotechnol. 10 (2011) 1715–1719.
[64] S. Mahdavi, S. Gharibzadeh, B. Ranjbar, M. Javan, Voltage-gated sodium channel gating modifiers: valuable targets for multiple sclerosis treatment, J. Neuropsychiatry Clin. Neurosci. 23 (2011) E17.